Journal of Colloid and Interface Science 690 (2025) 137333

Contents lists available at ScienceDirect

Journal of Colloid And Interface Science

journal homepage: www.elsevier.com/locate/jcis

Regular Article

A supported lipid bilayer to model solid-ordered membrane domains

Sally Helmy [a,b,1], Paola Brocca [a], Alexandros Koutsioubas [c], Stephen C.L. Hall [d], Luca Puricelli [e], Pietro Parisse [f,g], Loredana Casalis [f,*], Valeria Rondelli [a,*]

[a] Department of Medical Biotechnology and Translational Medicine, Università Degli Studi di Milano, Milano, Italy
[b] Biophysics Group, Physics Department, Faculty of Science, Ain Shams University, Cairo, Egypt
[c] Julich Centre for Neutron Science (JCNS) at Heinz Maier-Leibnitz Zentrum (MLZ), Forschungszentrum Julich GmbH, Garching, Germany
[d] ISIS Neutron and Muon Source, Rutherford Appleton Laboratory, Didcot OX11 0DE, UK
[e] Area Science Park, 34149 Padriciano, TS, Italy
[f] Elettra Sincrotrone Trieste, Basovizza, TS, Italy
[g] CNR-IOM, Basovizza, TS, Italy

HIGHLIGHTS

- A mimic for solid-ordered rafts based on saturated DMPC phospholipid has been created and characterized.
- The chosen lipid mixture shows a coexistence of S_o and L_α domains.
- Complementary physical techniques assess features and structuring of the mimic membrane.

GRAPHICAL ABSTRACT

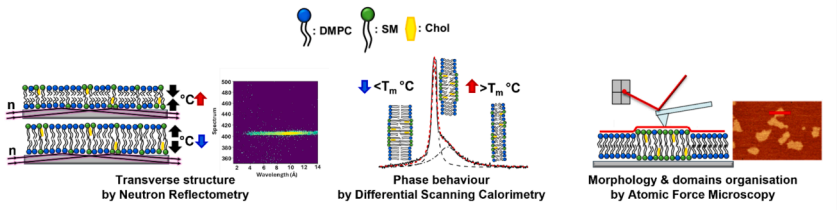

ARTICLE INFO

Keywords:
Neutron reflectometry
Differential scanning calorimetry
Atomic force microscopy
Lipid membrane
DMPC
Sphingomyelin
Cholesterol

ABSTRACT

Membrane models are widely used to mimic the behaviour of native plasma membranes and to simulate interactions occurring at their interface. Such models can be built up with different molecular compositions, ranging from single phospholipids to more complex, heterogeneous mixtures of phospho- and sphingo-lipids, possibly enriched with cholesterol and proteins. In particular, mixing different lipids and cholesterol is instrumental to promote the formation of phase-separated, ordered domains, which resemble the structure of lipid rafts, specialized functional domains of real membranes. According to the specific lipid composition, physical characteristics of the rafts can be tuned, such as fluidity, strongly related to membrane biological activity. Here, we introduce a novel three-component membrane model constituted by the mixing of a saturated phospholipid, 1,2-dimyristoyl-*sn-glycero*-3-phosphocholine (DMPC), sphingomyelin and cholesterol to mimic the presence of solid ordered rafts and to study their behaviour. Differential scanning calorimetry, neutron reflectometry, and atomic force microscopy were synergistically applied to gain information on the membrane's transverse and lateral organization, as well as on its thermotropic behaviour. The membrane model benefits from the use of DMPC, a lipid (i) characterized by an accessible transition temperature; (ii) saturated; (iii) fluid at physiological temperature and (iv) commercially available in both protiated and deuterated forms. The proposed model, along with the wide range of biophysical techniques employed, constitutes an ideal system to study the molecular

* Corresponding authors.
[1] Present address: Biophysics Group, Physics Department, Faculty of Science, Ain Shams University, Cairo, Egypt.

https://doi.org/10.1016/j.jcis.2025.137333
Received 25 November 2024; Received in revised form 11 March 2025; Accepted 13 March 2025
Available online 14 March 2025

mechanisms and the physical properties that govern membrane functions, such as molecular signalling and membrane trafficking.

1. Introduction

Complex model bilayers are required to mimic specific membrane portions and domains with a distinct molecular composition and distribution, present in native membranes [1]. Lipid rafts, in particular, are an example of membrane domains of high biological significance, featuring a different fluidity with respect to the surrounding membrane (hence the name 'rafts') [2–7], and responsible for several physiological functions [7,8]. The occurrence of lipid rafts is due to the preferential co-localization of molecules such as cholesterol, sphingolipids and saturated lipids [2,4,9], forming highly ordered domains ranging in size from the nano- (10–200 nm) to the microscale (>300 nm) [7]. Lipid rafts are surrounded by a fluid-disordered matrix [7,8]. Their time persistence is highly variable. Rafts are formed as a consequence of liquid–liquid separation of lipids with different acyl chain length and saturation level into the membrane matrix, the driving force being preferential lipid-lipid or lipid-protein interaction, engaging a collective behaviour [10]. Sterols, with their flat and rigid structure, are well known to play a crucial role in liquid ordered phase formation [10,11], with higher preference of co-localization with sphingomyelins [12]. Proteins might be temporarily associated to lipid rafts, acting as initial players of interaction, driving cell–cell communication, budding, signal transduction, and cell polarization among other processes [13–16]. On the other hand, rafts are dynamic entities: their characteristics and persistence are highly influenced by the environmental conditions and by events occurring at cell surface as cholesterol homeostasis or lipid oxidation [17–19]. There is still great debate on the genesis, persistence time and peculiarities of rafts in living cells [20,21], and this is the reason why model systems are of primary importance in the field, allowing to understand from simpler systems what are the driving forces ruling the complex plasma membrane collective behaviour in physiological environment. The creation of suitable raft-like models to assess the specificity of molecular interactions, while controlling the composition and distribution of components both in the lateral and the cross-sectional directions through a wide range of complementary, biophysical techniques, is therefore of utmost importance.

The detection of rafts in model system requires a good synergy of short-range, i.e. microscopy (optical and/or force) techniques [22–26], and long-range scattering and reflectivity techniques. X-rays and, remarkably, neutrons have been proved to be excellent tools to spot rafts formation and their structural/dynamical characteristics, having the big advantage of leaving the system unperturbed and thus providing unique information on unperturbed systems [27–30].

A good model for mimicking lipid rafts is a ternary lipid mixture consisting of two different melting temperature lipids plus cholesterol. Experimental and theoretical models were developed and optimized for investigating the origin of domains formation and the required conditions for phase separation [20,31,32],studying the preferential co-localization within the rafts [33,34], and understanding the driving forces regulating membrane proteins-plasma membranes interaction [35–37].

Among others, well-exploited supported or bulk models are based on the mixing of unsaturated low T_m phospholipids with the high T_m sphingolipid sphingomyelin (SM) and cholesterol (Chol) [38,39]. 1,2-dioleoyl-*sn-glycero*-3-phosphocholine (DOPC) phospholipids have a very low gel-to fluid transition temperature (T_m = -16.5 °C) [40], so they form a fluid phase at room temperature. The mixture introduced above therefore presents a coexistence of liquid disordered (L_α) and liquid ordered (L_o) domains. Among others, our group has extensively worked with this membrane mimic, demonstrating first the occurrence of phase-separated, disordered-ordered domains, and then challenging the system to study the localized interaction with macromolecules/vesicles, by means mainly of atomic force microscopy (AFM) [35,36,41].

Beside the L_o domains, solid ordered (S_o) domains are also gaining increased importance in the rationalization of the biological membrane's functionality [42,43]. S_o domains are stable, organized structures that play a relevant role in recruiting specific lipids and proteins, allowing for the organization/segregation of different components within the membrane for intracellular transport, assembly of signalling platforms and for the integrity of the cell [42,43]. S_o domains are also supposed to play a role in maintaining contacts between the different organelles, facilitating inter-organellar crosstalk and lipid transfer [43]. S_o domains crystallize and grow/decay until they reach a critical size, thus corresponding to the definition of the lipid rafts as laterally mobile associating/dissociating entities [44]. The transition of the S_o domains to the liquid phase has low occurrence probability, requiring longer time scales with respect to L_o domains, being thus compatible with specific cellular events as protein–protein transient interactions which require timeframes ranging from minutes to hours to occur [42,45,46]. The gel state of lipids in S_o domains provides localised membrane stiffening, suggesting their relevance in defence mechanisms [47,48] not assured by the sole L_o domains. They contribute in fact to membrane homeostasis by regulating the membrane's physical properties, such as its fluidity and thickness, through the action of "sense-and-response" regulators [43].

Therefore, we concentrated here on proposing a novel, raft-like membrane mimic, presenting S_o domains. In particular, we paid attention to design our system in a way to be widely accessible to advanced physical techniques, merging different spatial and time scales. Towards this end, we introduced 1,2 dimyristoyl phosphatidylcholine (DMPC) as a substitute of DOPC, used in our previous L_o domains membrane model. DMPC shows in fact saturated fatty acid chains and is therefore characterized by a quite higher T_m (24 °C) [49], being anyway fluid at the physiological 37 °C. In addition, it has already been widely used as a matrix for model membranes [50–52], being its melting temperature accessible by a wide range of techniques such as differential scanning calorimetry (DSC) [53–63] and AFM [35,36,64–67]. Another important advantage is the commercial availability of its deuterated form, that makes it a good candidate to perform neutron-based studies [35,68–70]. In particular, we developed and characterized a complex membrane model composed of DMPC/SM/Chol in the form of a supported lipid bilayer (SLB), displaying 'raft-like' domains evolving with temperature. All the 3 molecular constituents are shown to be exposed on the outer surface, thus creating a peculiar interface accessible to the incoming macromolecules. To characterize the membrane, we exploited here complementary NR, DSC, and AFM techniques, profiting from the use of both the deuterated and protiated forms of the DMPC phospholipid, according to the requirements for each technique. We describe the membrane phase behaviour and transverse structure at different temperatures, while investigating the surface morphology of this lipidic mixture for the first time. This platform is intended to be used as a S_o raft-rich planar membrane mimic, whose structural features can be accessed by a variety of state-of-the-art techniques to investigate the molecular details of macromolecules interaction with plasma membranes.

2. Materials and methods

1,2-dimyristoyl-*sn-glycero*-3-phosphocholine (DMPC) and 1,2-dimyristoyl-d54-*sn-glycero*-3-phosphocholine (d_{54}DMPC) were purchased from Avanti Polar Lipids Co. Sphingomyelin (SM) from egg ≥ 95 %, cholesterol (Chol) ≥ 99 % and phosphate buffered saline (PBS) were

purchased from Sigma Aldrich. $D_2O \geq 99$ % purity was purchased from Sigma Aldrich.

2.1. Model membranes preparation

Different model membranes were obtained according to a standard protocol [71]. Briefly, individual powdered constituents were separately weighed and combined in the following molar ratios: DMPC, d_{54}DMPC, d_{54}DMPC:SM; 2:1, d_{54}DMPC:Chol; 2:0.15, d_{54}DMPC:SM:Chol; 2:1:0.15 and DMPC:SM:Chol; 2:1:0.15. Once combined, powdered lipids were dissolved in chloroform in glass pear-shaped flasks. Thin lipid films were deposited on the flasks surface while evaporating the chloroform by the continuous rotation of the flask. Full chloroform evaporation was then achieved under vacuum for 120 mins. Later, the deposited lipid films were put under gentle stream of humidified nitrogen for 60 mins to untangle the multilamellar stacks. According to their application and the requirements for each technique, the lipid films were then processed as described below.

For neutron reflectometry (NR), the lipid film of the deuterated raft d_{54}DMPC:SM:Chol; 2:1:0.15 membrane model -will be denoted here as dRaft- was hydrated with a 150 mM NaCl H_2O buffer to get a stock concentration of 30 mg/ml which was then freezed and thawed for 5 cycles, then extruded 51 times through double polycarbonate filters of 80 nm porosity using a manual extruder (LiposoFast, Avestin Inc.) to form large unilamellar vesicles (LUVs). Samples were stored at 37 °C above the T_m to guarantee the LUVs stability and were eventually diluted to a final concentration of 0.5 mg/mL just before incubation in the NR measurement cells for the supported lipid bilayer (SLB) deposition process.

For atomic force microscopy (AFM), the lipid film of the protiated raft DMPC:SM:Chol; 2:1:0.15 was hydrated with 100 mM NaCl buffer, obtaining an initial concentration of 1 mg/mL, then freezed and thawed for 5 cycles and extruded through polycarbonate membranes of 100 nm porosity using the Avanti Polar Lipids extruder, and stored at 40 °C. Just before incubation in the AFM measurement cell for depositing the SLB, the LUVs were further diluted in 100 mM NaCl and 10 mM $CaCl_2$ buffers according to the ratios 1:1:2 respectively, obtaining a final lipid concentration of 0.25 mg/mL.

For differential scanning calorimetry (DSC), the lipid films of d_{54}DMPC, d_{54}DMPC:SM; 2:1, d_{54}DMPC:Chol; 2:0.15 and d_{54}DMPC:SM:Chol; 2:1:0.15 were directly hydrated to 2 % concentration with PBS buffer (i.e. similar to the conditions used for preparing the final SLB deposition for NR as will be explained next) to form lamellar membrane structures, which were then freezed and thawed for 5 times. Another lipid film of DMPC:SM:Chol; 2:1:0.15 was instead hydrated in 100 mM NaCl (i.e. similar to the conditions used for the SLB deposition by AFM), forming lamellar membrane structures, then freezed and thawed for 5 times with no further processing or extrusion.

2.2. Deposition of the supported lipid bilayer (SLB) for NR and AFM

For NR, silicon substrates were cleaned by methanol, chloroform, ethanol and milli-Q water (by sonication for 10 min in each solvent) and, just before closing the cells, UV-Ozone cleaning for 30 min. The dRaft LUVs prepared in NaCl H_2O were injected onto the clean bare silicon substrate cell from which a reflectivity spectrum was previously measured such that the silicon oxide layer of the solid support could be characterised. dRaft LUVs were incubated in the presence of this clean surface within flow cell for 45 min at 37 °C [72,73]. During the LUVs incubation, reflectometry measurements at the 0.6° angle were recorded every 3 mins to study the kinetics of the SLB formation on the silicon support. After the 45 min of incubation, the excess unfused LUVs were flushed away by 20 mL of H_2O at a rate of 1.5 mL/min and then the solvent was changed to H_2O PBS. NR spectra were measured at 37 °C and 17 °C at the two incoming angles 0.6° and 2.3° for the supported dRaft bilayer in 3 solvent mixtures with different SLDs, namely; H_2O PBS, SiMW (Silicon Matched Water) PBS (i.e. a mixture of H_2O:D_2O; 62 %:38 % such that the scattering length density −SLD- is equal to that of Silicon) and D_2O PBS. Decreasing the temperature from 37 °C to 17 °C was achieved by reducing 2 °C every 10 mins and NR spectra were recorded in D_2O PBS at the intermediate temperatures of 31 °C, 25 °C, 21 °C. For comparison, another deposition of the same dRaft SLB composition was measured in a second cell in the same 3 solvent mixtures, only at 37 °C and 17 °C.

For AFM, the standard protocol for the vesicles fusion for obtaining a planar SLB was achieved by depositing 50 μL of the LUVs final concentration on a freshly cleaved mica substrate (Nano-Tec V-1 grade, 10 mm diameter, 0.15 − 0.21 mm thickness), incubated at 50 °C for 20 min, then slowly cooled down to 45 °C by 0.07 °C/s rate. The excess unfused vesicles were carefully washed away with NaCl buffer 100 mM. The SLB on mica was properly sealed in a temperature-controlled AFM cell, that was then cooled down to 17 °C by 0.02 °C/s rate, before starting imaging. Temperature was then increased by 0.02 °C/s rate and a set of AFM images at selected temperatures were acquired during the heating ramp while stopping for the membrane to stabilize at the chosen temperature checkpoints, passing by the membrane transition temperatures for imaging the SLB following the formation of the gel-domains.

2.3. Neutron reflectometry (NR) measurements and data analysis

NR provides information about the buried structure of the investigated sample along its transverse direction. In neutron-based experiments, deuterated phospholipids (here DMPC) are used to enhance the visibility of other protiated lipids (here SM and Chol) present in the lipid bilayer giving an estimation of their lateral/cross distribution [30,71] in the membrane. The NR measurements were performed on the Offspec vertical reflectometer at the ISIS Neutron and Muon Source, Oxfordshire, UK, in TOF mode, utilising both a constant resolution $\Delta q_z/q_z = 4$ % and projected 60 × 30 mm footprint on the sample, with incident wavelengths λ ranging between 1.5–14 Å, at two incoming angles θ of 0.6° and 2.3°. During the measurement, the reflectivity $R(q_z)$, which is the ratio between the intensities of the specular reflected and incident neutron beams, is measured as a function of the momentum transfer (q_z) perpendicular to the interface. The momentum transfer $q_z = \frac{4\pi sin\theta}{\lambda}$, where θ is the incident neutron beam angle and λ is the neutron wavelength. The information on the structural composition of the sample layers is thus given by the function $\rho(q_z)$ which is the Fourier transform of the scattering length density (SLD) profile $\rho(z)$ that depends on the coherent scattering length contributions (b_c) of N atoms within a molecular volume V_m, as given by the equation $SLD = \rho(z) = \frac{\sum_{i=1}^{N} b_c}{V_m}$. The reflectivity $R(q_z)$ is therefore related to the SLD by the equation; $R(q_z) \approx \frac{16\pi^2}{q_z^4}\left|\int \frac{d\rho(q_z)}{dz} e^{iq_z z} dz\right|^2$. In cases where domains smaller than instrument's coherence length are present on sample surface, the measured reflectivity represents an average of the contributions across the interface illuminated by the beam [74]. Here, as observed by AFM (see results section), domains are present, whose size is substantially below the neutron beam coherence length (tens of microns). Therefore, here, layers SLD was accounted for as laterally uniform. The NR data were analysed by the open-source Python script *Anaklasis* [75]. It allows the study of the specular neutron reflectivity by fitting the model NR curves against the experimental data sets. Therefore, it enables the calculation of the parameters characterizing the different layers constituting the model membrane, such as the thickness, SLD, roughness and solvent penetration. The approach used to reduce the overall model uncertainty, was applied by simultaneously fitting the different NR curves of the dRaft SLB from the solvent-contrast-variation series [76,77]. The NR spectra were fitted concurrently in the 3 mixtures of H_2O and D_2O with different SLD, assuming the subsequent layers to be: silicon oxide (SiO_2), thin water layer, the SLB membrane model as (inner

heads/inner tails/outer tails/outer heads) and the outer bulk solvent layer. For the estimation of confidence intervals of the fitted model parameters and for identifying any potential correlations between free parameters, we performed a Bayesian MCMC sampling of the system as implement in the Anaklasis package [75]. In the SLD profile plots the 95 % confidence intervals are depicted by lighter color shade around the mean curve. Preliminary analysis of NR data indicated the best fits were achieved with symmetric lipid distributions on each leaflet of the bilayer. All subsequent analysis therefore constrained the bilayer to be symmetric in composition to reduce the parameter space.

2.4. Differential scanning calorimetry (DSC) measurements

Differential scanning calorimetry (DSC) was performed to investigate the thermotropic behaviour of the different membrane models, in order to discriminate their different phase behaviours and the separate effect of each component when being mixed with the d_{54}DMPC. DSC was carried out using a non-commercial double differential scanning calorimeter instrument (MASC) manufactured in the laboratories of the Istituto per i Processi Chimico-Fisici (IPCF) at the CNR of Pisa, Italy [78] that can access temperatures ranging from −20 to 200 °C with a temperature sensitivity of 0.002 °C, and power sensitivity of ±30 μW. This calorimeter consists of 2 identical cells where 2 glass capillaries are used, one containing the sample solution and the other with the water reference. The specific heat capacity *Cp* of the sample is therefore measured by computing the difference between the power supplied to the 2 measuring cells due to a controlled change of temperature over time. The model membrane samples were submitted to temperature cycles ranging from 5 °C to 60 °C at a scan rate of 1 °C/3 min, in cooling and heating modes. At the beginning of the measurement, a 60 mins isotherm was set at 60 °C to provide the sample and the instrument enough time to reach the thermal equilibrium. Afterwards, isotherms of 3600 *sec* were set before each cooling and heating cycles.

2.5. Atomic force microscopy (AFM) measurements

Atomic force microscopy (AFM) was performed to monitor the temperature-induced phase transition of the raft SLB model and to visualise the phase separation occurring in the membrane fluid phase. To prepare the raft model for the AFM imaging, protiated DMPC was used instead of the deuterated DMPC due to its better convenience for this kind of imaging experiment where the protiated lipids are commonly employed [64,67,79,80]. Incubation and imaging of the SLB was performed in a temperature-controlled cell on the AFM microscope (Cypher VRS1250 from Oxford instruments, Asylum Research), at different selected temperatures, passing through the transition temperatures of the model membrane. For the image acquisition, micro cantilever (BL-AC40TS-*C*2 from Olympus) with nominal resonant frequency f=110 kHz, and spring constant k=0.09 N/m was used in the AC liquid imaging mode. Images were acquired with 512 × 512 points & lines at 1.45 Hz scan rate. Image analysis was performed by Gwyddion software V.2.58 and Origin Pro2023b.

3. Results and discussion

3.1. Transverse structure of the lipid raft mimic by neutron reflectometry (NR)

Creating supported lipid bilayers (SLB) models with a given lipid composition and leaflet asymmetry, designed to replicate specific cell membrane conditions, is a complex task, and requires precise structural and morphological characterization. In particular, it is critical to understand the distribution of the model membrane's single components both transversely and laterally. Towards this goal, we applied NR to investigate the transverse distribution of the components in the surface-supported dRaft model. Specifically, the membrane was made of d_{54}DMPC:SM:Chol 2:1:0.15 mol, where deuterated DMPC was used to distinguish it from cholesterol (Chol) and sphingomyelin (SM), inside the phospholipid leaflets, according to their different scattering length density (SLD) values, as presented in Table 1.

The time necessary for the formation of a SLB from the LUVs, as well as the final distribution of components within the two membrane leaflets, is substantially dependent on the lipidic composition, lipid-substrate, and lipid-lipid interaction, as well as on the different lipid packing phases [85]. The kinetics of the dRaft SLB formation onto the Si substrate was found to be very fast as a high intensity neutrons reflection was observed already at the first NR collection, roughly 3 mins after the LUVs injection into the measuring cell (see Fig. S1), to indicate the formation of the dRaft SLB. The dRaft SLB deposition was tested by injecting the dRaft LUVs, suspended in 150 mM NaCl buffer and incubated onto the silicon (Si) face inside the measuring cell at 37 °C for 45 mins, while neutrons reflected on the detector at 0.6° were collected every 3 mins, to follow the LUVs' fusion process. The reflected intensity at 0.6° has remained stable during the full incubation time and after flushing any excess of unfused liposomes. Consequently, this indicates the highly efficient and rapid fusion of the current dRaft LUVs to form SLB, in comparison to another previously studied GM1-loaded mimic where the full interval of 45 mins was necessary for the LUVs to fully fuse on the Si support forming the SLB [71].

After fusion, full reflectivity curves were collected from the deposited membranes at varying temperatures in the 3 H_2O-D_2O mixtures with different SLDs. The experiment was repeated twice, to check for reproducibility and it was found that both SLB depositions had a very high coverage (97 % in one case, and 95 % for the second membrane deposited).

Detailed fit of the reflectivity spectra of the dRaft SLB at 37 °C and 17 °C, respectively, by anaklasis software and the corresponding SLD profiles in the 3 H_2O-D_2O mixtures are shown in Fig. 1. Best fit parameters are reported in Table 2 (for the 1st SLB deposition) and in the SI, Table S1 (for the 2nd SLB deposition, respectively).

Data analysis unveils that the membrane SLD and thickness are symmetric with respect to membrane centre, indicating that Chol and SM symmetrically arrange within the two d_{54}DMPC leaflets matrix. Specifically, hydrophobic portion was found to be $4.25{\cdot}10^{-6}$ Å^{-2} at 37 °C and $4.57{\cdot}10^{-6}$ Å^{-2} at 17 °C, in full agreement with the theoretical SLD of the used lipid mixture. We then followed membrane stability and transverse structure at varying temperatures. Between the two deposited membranes, we selected the first dRaft SLB (the one having a better support coverage deposition) to collect reflectivity at the intermediate temperatures of 31 °C, 25 °C, and 21 °C. Since in this temperature range the membrane undergoes the melting phase transition and is therefore expected to be unstable, reflectivity spectra were collected in one solvent only, namely D_2O, to have a better contrast from the protiated components (lipid heads, SM and Chol). The corresponding spectra are reported in Figs. S2 and S3, together with their best fits.

The SLD profiles obtained from the best fittings lines at all investigated temperatures are shown in Fig. 2**a.** Moreover Fig. 2**b** highlights the correspondence between the SLB heads and tails regions on the SLD profiles as derived from the data fitting and serves as a guide for data interpretation. The corresponding best fit parameters for the dRaft SLB layers' thicknesses, SLDs and solvent penetration values at the different temperatures are reported in Table 2**.**

As appears from Table 2, upon lowering the temperature, the overall thickness of the SLB increased, as expected, mainly due to the thickening of the hydrophobic alkyl chains. In particular, the full bilayer thickened from 43 Å to 50 Å upon decreasing the temperature from 37 °C to 17 °C. In the same temperature interval, the hydrophobic chains contribution went from 27 Å to 34 Å. The SLD of the alkyl chains, inversely proportional to the chains molecular volume V_{Tails}, changed accordingly from 4.25 ± 0.01 e-6 Å^{-2} to 4.57 ± 0.02 e-6 Å^{-2}. This is in agreement with a transition to the gel phase, which has been already reported also in the presence of low concentrations of cholesterol [81]. According to

Table 1
Partial molecular volumes and SLDs of the model membrane's single components at temperatures high above their transition temperatures (T_H), and low below their transition temperatures (T_L), respectively, as calculated from literature data [81–84].

Component	Chemical formula		V_L (x = 0) (Å^3)	x_c	V_L (x < x_c) (Å^3)	V_C (x < x_c) (Å^3)	V_{Head}, V_{Tail} (Å^3)	SLD_{Head}, SLD_{Tail} (e-6 Å^{-2})
d_{54}DMPC (T_H)	Head: $C_{10}H_{18}NO_8P$	Tail: $C_{26}D_{54}$	1099.4	0.240	1099.6		319, 780.4	1.88, 6.83
d_{54}DMPC (T_L)			1045				319, 726	1.88, 7.34
SM (T_H)	Head: $C_8H_{19}N_2O_6P$	Tail: $C_{31}H_{62}$		0.269	1233.1		324, 909.1	1.37, −0.28
SM (T_L)			1175.6	0.200	1175.6		324, 851.6	1.37, −0.30
Chol (T_H)	$C_{27}H_{46}O$					575.2		0.23
Chol (T_L)						621.8		0.21

V_L is the partial molecular volume of the lipid alone or when mixed with cholesterol, V_{Head} is the partial molecular volume of the lipid head group, V_{Tail} is the partial molecular volume of the lipid tail and V_C is the partial molecular volume of cholesterol, x_c is the mole fraction of cholesterol. SLD_{Head} is the scattering length density of the lipid head, SLD_{Tail} is the scattering length density of the lipid tail, while the volume and SLD for cholesterol are calculated for the molecule as a whole.

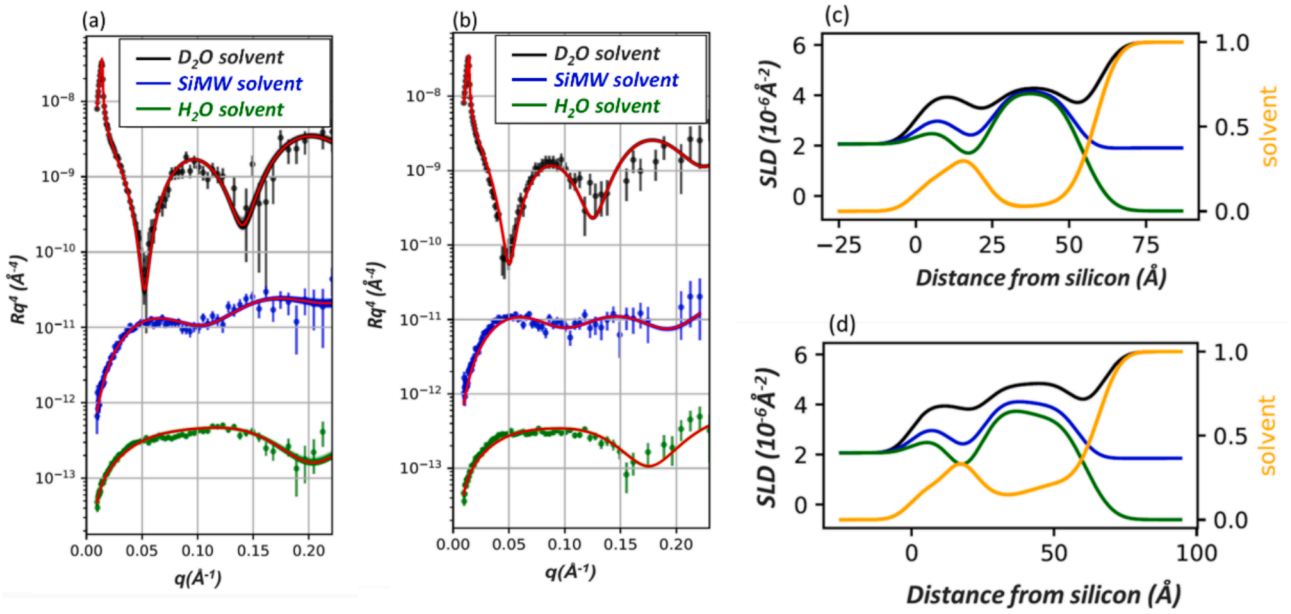

Fig. 1. Best fittings for the NR spectra of the main dRaft SLB at 37 °C and 17 °C. Best fit (lines) for the NR spectra (dots) of the dRaft SLB at 37 °C (a) and 17 °C (b) in the 3 water solvents (D_2O in black, SiMW in blue and H_2O in green). The H_2O and SiMW reflectivity curves are shifted down on the vertical axis, with respect to D_2O reflectivity, each by a factor 10^{-3}, for the sake of clarity. Solvent penetration percentage is shown in yellow (right axis) together with the respective SLD profiles (left axis) at 17 °C (c) and 37 °C (d). (For interpretation of the references to color in this figure legend, the reader is referred to the web version of this article.)

extensive literature [86], as the lipid polar portions are fully hydrated, they are assumed to have a constant volume V_{Head} in the whole temperature range investigated. Upon lowering the temperature, the membrane layers' solvent penetration was also found to increase by roughly 12 %, in total volume. Such an increase is intended to be associated to reduced volume per lipid, with thicker chains and smaller area per headgroup, going from the fluid to the gel phase, which causes a lateral contraction of the area occupied by the lipids, leaving more volume free to water penetration. The rising of similar defects will be seen by AFM images after the first jump to low temperature (see Fig. 6**a** below).

As already mentioned, the dRaft SLB deposition experiment was performed in duplicate, to test for reproducibility, where both membranes have been found to present a symmetric deposition of components between the two leaflets. The NR spectra relative to the second deposition in the 3 H_2O-D_2O mixtures at 37 °C and 17 °C presented very similar results to the first deposition, as shown in Fig. S5, together with best fitting parameters presented in Table S1. Again, data analysis has showed a symmetrical distribution of the SLB components with similar SLD profiles, and an increase in the total SLB thickness from 44 Å at 37 °C to 52 Å at 17 °C.

We would like to remind the relevance of tracking the components transverse distribution within SLB. In many biological/medical applications, where cells are exposed to drugs, nanovesicles, or interacting macromolecules, it is in fact extremely important to determine the exact composition of the leaflet exposed to the outside bulk water, facing the incoming interacting molecules. The different lipid species are expected to cooperatively tune the interactions with the incoming molecules [35]. In the current case, we witnessed a symmetrical distribution of the dRaft SLB components, which is in contrast with former neutron reflectometry measurements performed on bilayers of different composition [87,88]. For example, the presence of the GM1 ganglioside, asymmetrically arranged in the membrane, induced a "non-spontaneous", asymmetric distribution of cholesterol between the bilayer leaflets [87], as a consequence of the direct, specific molecular interactions between cholesterol and GM1 itself.

3.2. Phase behaviour of the lipid raft mimic by differential scanning calorimetry (DSC)

The thermodynamics and thermotropic behaviour of the 4 membrane sub-models in the multilamellar state were investigated by performing DSC. Single component, double and ternary lipid mixtures, namely d_{54}DMPC, d_{54}DMPC:SM 2:1, d_{54}DMPC:Chol 2:0.15 and d_{54}DMPC:SM:Chol 2:1:0.15, −where proportions are expressed in terms of molar ratios- were identified in order to go from simple systems to the final complex dRaft model studied in the NR experiments. The DSC cooling thermograms of the 4 model membranes in PBS buffer are shown

Table 2
Best fit parameters for the NR curves of the dRaft model membrane collected in 1 to 3 contrast waters at different temperatures of 37, 31, 25, 21 and 17 °C, respectively, while cooling. **Fig. S4** shows the confidence intervals for the fitting's parameters.

Temperature (°C)	*dRaft SLB layers*	*Thickness (Å)*	*Full Thickness (Å)*	*SLD (10^{-6} Å^{-2})*	*Solvent penetration (% vol)*	*Roughness with previous layer (Å)*
37	Heads inner	8 ± 1	43	1.70 ± 0.1	15 ± 1	5 ± 1
	Tails inner	13 ± 1		4.25 ± 0.1	2 ± 2	5 ± 1
	Tails outer	14 ± 1		4.25 ± 0.1	4 ± 1	5 ± 1
	Heads outer	8 ± 1		1.70 ± 0.1	20 ± 3	5 ± 1
31	Heads inner	8 ± 1	44	1.70 ± 0.4	16 ± 4	5 ± 1
	Tails inner	14 ± 1		4.32 ± 0.4	5 ± 3	5 ± 1
	Tails outer	14 ± 1		4.32 ± 0.3	10 ± 2	5 ± 1
	Heads outer	8 ± 1		1.70 ± 0.3	24 ± 3	5 ± 1
25	Heads inner	8 ± 1	46	1.70 ± 0.3	18 ± 5	5 ± 1
	Tails inner	15 ± 1		4.44 ± 0.4	9 ± 6	5 ± 1
	Tails outer	15 ± 1		4.44 ± 0.4	14 ± 6	5 ± 1
	Heads outer	8 ± 1		1.70 ± 0.3	27 ± 4	5 ± 1
21	Heads inner	8 ± 1	48	1.70 ± 0.3	19 ± 5	5 ± 1
	Tails inner	16 ± 1		4.51 ± 0.3	11 ± 5	5 ± 1
	Tails outer	16 ± 1		4.51 ± 0.3	19 ± 5	5 ± 1
	Heads outer	8 ± 1		1.70 ± 0.3	29 ± 3	5 ± 1
17	Heads inner	8 ± 1	50	1.70 ± 0.3	22 ± 4	6 ± 1
	Tails inner	17 ± 1		4.57 ± 0.1	14 ± 5	6 ± 1
	Tails outer	17 ± 1		4.57 ± 0.2	21 ± 4	6 ± 1
	Heads outer	8 ± 1		1.70 ± 0.3	31 ± 2	6 ± 1

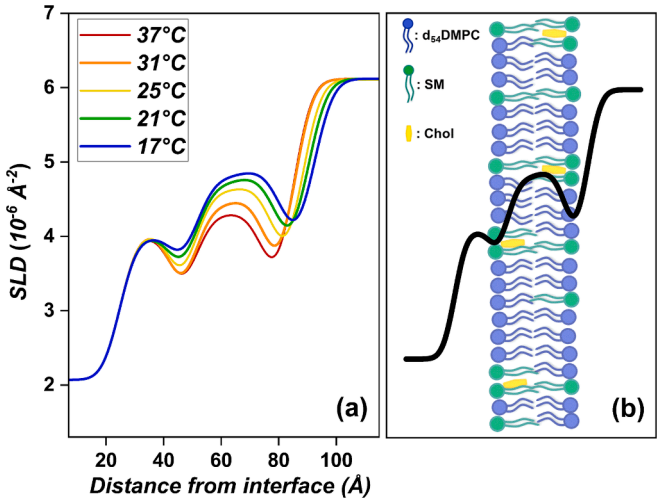

Fig. 2. SLD profiles of the main dRaft SLB at all measured temperatures in D_2O. The SLD profiles of the dRaft SLB show (a) SLD profiles of the dRaft membrane at 37 °C in red, 31 °C in orange, 25 °C in yellow, 21 °C in green, and 17 °C in blue. (b) Graphic sketch to guide the eye in assessing the correspondence between hydrophilic head and hydrophobic tail regions of the SLB and its SLD profile. These analyses indicate that the deposition of such a complex biomimetic membrane model is feasible, allowing the fabrication of a single supported bilayer which is symmetric in composition across the tested temperatures, and shows a thinning with increased temperature. Note that while three bulk solution contrasts were measured at 37°C and 17°C and intermediate temperatures were measured only D_2O, only D_2O data are shown for clarity. (For interpretation of the references to color in this figure legend, the reader is referred to the web version of this article.)

in Fig. 3. Indeed, the dRaft model demonstrated a complex behaviour during its broad transition. To allow easier thermograms comparison, data are reported as ΔCp, that is the excess Cp registered during the phase transitions, with respect to the systems' Cp before and after the phase transition.

The main phospholipid used in this dRaft model is d_{54}DMPC which is known to have a T_m around 19 °C, about 4 °C lower than the protiated DMPC [89,90]. It is also noteworthy to mention that the calorimetric data on deuterated d_{54}DMPC based systems are actually scarce in the literature. The main transition of d_{54}DMPC in PBS buffer (Fig. 3 black thermogram) appeared indeed to be in very good agreement with values stated for the lamellar phase of deuterated DMPC in literature [89], with a very sharp transition peak (full width at half maximum, FWHM = 0.3) at $T_m = 18.9 \pm 0.1$ °C, with a transition enthalpy $\Delta H = 35 \pm 1$ J/g and a maximum heat capacity $\Delta Cp_{max} = 94 \pm 1$ J/gK. Regarding the phase behaviour of this single component d_{54}DMPC model, there should be two main phases depending on the T_m: the gel phase designated as tilted gel or ripple gel phase (P_β or $P_{\beta'}$), below the stated T_m, and the liquid crystalline (L_α) phase above the T_m [91].

Regarding the effect of adding sphingomyelin (SM) to d_{54}DMPC, previous studies have shown that the SM bilayers alone exhibit a main transition centred around $T_m = 38$ °C with a peak broadness of 4 °C. This broadening is expected due to the variation in chain lengths found in the naturally extracted egg SM [92]. Earlier research has also showed that, due to their similar hydrogen bonding properties, SM can almost ideally mix with DMPC [33]. Here the thermogram of d_{54}DMPC:SM 2:1 model (Fig. 3 green), shows a broad enthalpic peak with a T_m centred at 26 °C (FWHM = 4.2 °C) with ΔCp max reduced to 6.2 ± 0.1 J/gK. The tail with associated low enthalpy observed at higher temperature possibly points to a coexisting minor contribution of SM enriched domains, as supported by previous observation on binary lipid mixtures [93]. Considering the melting temperature of the main peak, shifted by 7 °C from the very sharp transition at 18.9 ± 0.1 °C observed for the pure d_{54}DMPC and by about 12 °C from T_m of egg SM, a very good agreement is found with the estimated average temperature obtained for highly mixed DMPC:SM 2:1. Moreover, the measured ΔH of 34 ± 1 J/g (total lipid) is in good agreement with a theoretical weighted average enthalpy for the d_{54}DMPC:SM 2:1 model, pure SM having an enthalpy of transition ΔH, of 30 J/g [94], that yields ΔH of 33.3 J/g.

Then, regarding the cholesterol (Chol) effect, the extensive literature on the phase diagrams of binary mixtures consisting of a pure DMPC and Chol between about 5 mol% and 30 mol% [95–97], indicates the coexistence of two phases. Above T_m, a liquid-ordered (L_o) phase and a

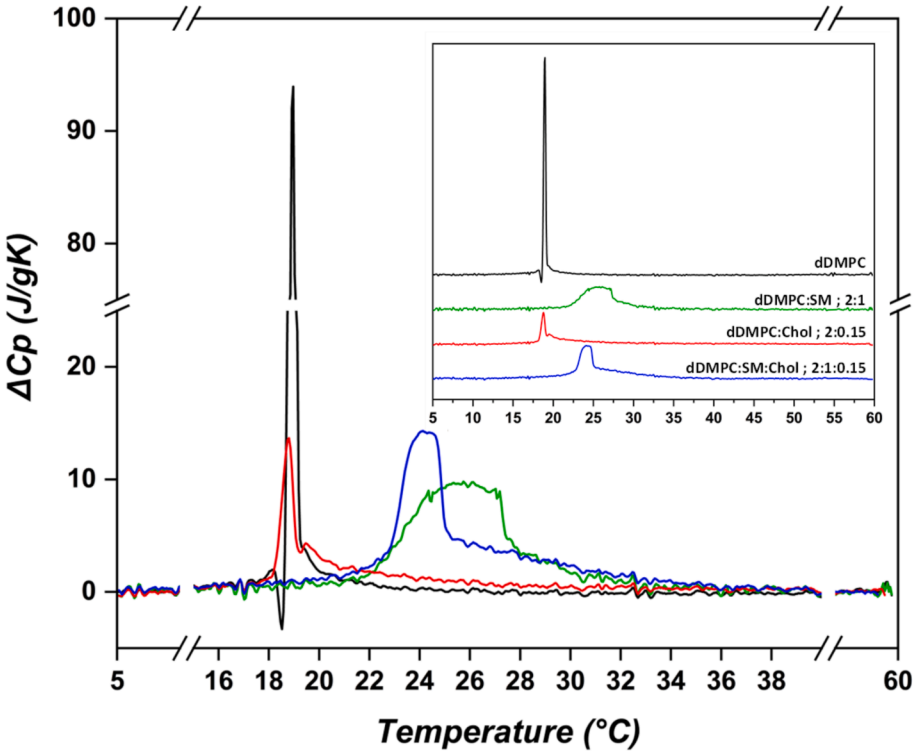

Fig. 3. DSC thermograms of lamellar systems of the dRaft model membrane and its separate components. d_{54}DMPC (black), d_{54}DMPC:SM; 2:1 (green), d_{54}DMPC:Chol; 2:0.15 (red) and d_{54}DMPC:SM:Chol; 2:1:0.15 (blue). Data were collected at a scan rate of 1 °C/3 min, in cooling mode. The insert shows the full spectra shifted on the y-axis for better visualisation. Data are reported as ΔCp, that is the excess Cp registered during the phase transitions, with respect to the systems' Cp before and after the phase transition. (For interpretation of the references to color in this figure legend, the reader is referred to the web version of this article.)

liquid-disordered (L_α) fluid phase are found to coexist, while upon decreasing the temperature below the T_m, a rigid gel phase (also indicated as solid ordered S_o) is found still coexisting with the L_o phase [95,97]. It was also previously verified that upon mixing cholesterol with a pure phosphatidylcholine phospholipid, cholesterol slightly reduces the main T_m of the pure phospholipid system and largely reduces

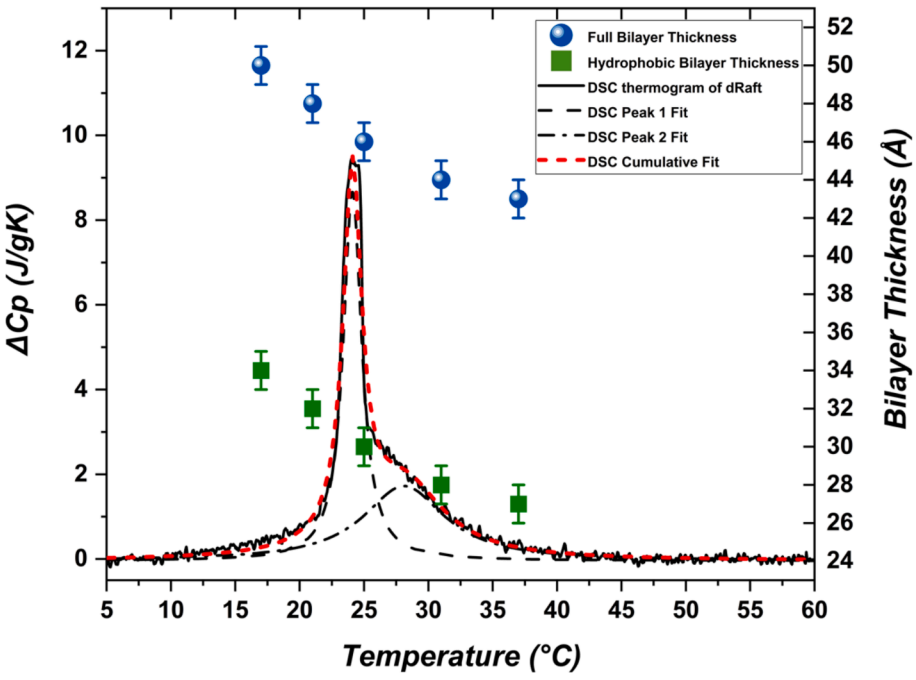

Fig. 4. Deconvolution of the DSC thermogram of the dRaft model membrane. Data were collected with a scan rate of 1 °C/3 min, in cooling mode. Overlaid points correspond to the SLB thicknesses observed by NR upon decreasing temperatures. Blue circles show the full bilayer thickness, green squares show the hydrophobic bilayer thickness measured by NR while cooling at temperatures of 37, 31, 25, 21, 17 °C. (For interpretation of the references to color in this figure legend, the reader is referred to the web version of this article.)

the ΔH in an amount dependent fashion [98–100]. The ΔH of the currently investigated d_{54}DMPC:Chol 2:0.15 mixture (Fig. 3 red thermogram), has indeed reduced to 22 ± 1 J/g. The shape of the enthalpic peak was also no longer symmetric in presence of cholesterol, indicating a phase inhomogeneity. Specifically, the peak seemed to be the composition of two peaks, indicating that lipids in different states were undergoing the transition at different temperatures. A sharp transition of low-cholesterol L_d domains appeared at a temperature of 18.7 ± 0.1 °C, slightly lower than that of the pure phospholipid, in addition to another broad transition peak centred at higher temperature of 19.4 ± 0.1 °C, involving higher-cholesterol contents domains. The sharper peak occurring at lower temperature very similar to the pure d_{54}DMPC T_m (18.9 ± 0.1 °C) is therefore assumed to be associated to the phospholipid domains containing very low molar fractions of cholesterol.

The ternary mixture of the dRaft lamellae d_{54}DMPC:SM:Chol 2:1:0.15, has exhibited a rather complex phase behaviour, with a thermogram, reported in Fig. 3 (blue thermogram), showing a main enthalpic peak centred around 24 °C, followed by a very broad peak extending until 40 °C. It is rather clear that this mixture exhibits a large enthalpic peak area. This indicates the tendency of components to separate, at high temperatures, into more-rigid domains, plausibly enriched in sphingomyelin and cholesterol, while the phospholipids enriched regions contribute mainly to the less rigid domains [101], where cholesterol is the agent causing the phase separation. The total transition enthalpy (ΔH) of the dRaft lamellae was found to be 38 ± 1 J/g, as close to the theoretical weighted average contribution of the main components.

To evaluate the contribution of the two phases, peaks deconvolution into 2 distinct Lorentzian curves was performed as shown in Fig. 4. The sharp main first transition peak at 24 °C was associated to a deconvoluted peak with FWHM = 1.7 °C. The increase in T_m and width broadening of this peak compared to the pure d_{54}DMPC could be attributed to the presence of SM, as for the binary mixture, though in low proportion. On the other hand, the bigger broadness of the second contribution peak centred at around 28 °C with FWHM = 7.5 °C suggested the multiform molar composition DMPC/SM/Chol of the more ordered/gel fraction of the system. The shift of the melting event to a temperature higher than that of the d_{54}DMPC/SM binary mixture, accredits domains that could be highly enriched with SM above the 2:1 ratio. According to phase diagrams of other related ternary mixtures [102], the current raft composition could be assumed to have a coexistence of a liquid-disordered L_α phase with a rigid-ordered gel S_o phase.

It could be observed that the effect of cholesterol addition, even in low proportion, has caused the dropping of the ideal mixing of the d_{54}DMPC/SM binary mixture to a phase separated mixture. The conserved ΔH with respect to the binary mixture denotes that the L_o phase is not present (differently than in the investigated d_{54}DMPC:Chol 2:0.15 system). All lipid chains undergo phase change from gel to fluid states but pertaining to two different domains, enriched, or depleted in SM, as the transition occurs in two steps. Consequently, above the first (24 °C) melting, the thermogram has showed a large temperature interval of gel-fluid coexistence (from about 25 to 35 °C), while at 40 °C the system has entirely transitioned to a fluid phase. The colocalization of cholesterol in the SM enriched/depleted domains or at the domains border is un-demonstrated here, however speculation from the literature would suggest the preferential cholesterol co-localization with sphingomyelin (SM) even in the presence of a phospholipid with an equal acyl chain order [103].

Significant comparisons between thermodynamical and structural insights on the bilayer allow understanding the ternary mixture features. Fig. 4 also shows the correlation between the changes in the bilayer thicknesses and the thermogram of the dRaft model. The full and hydrophobic bilayer thicknesses obtained from the NR measurements at the investigated temperatures of 37 °C, 31 °C, 25 °C, 21 °C and 17 °C, represent the thickening of the bilayer upon reducing the temperature along the fluid-to-gel chains phase transition. NR effectively measures the weighted average thicknesses of any coexisting regions across a phase transition. Therefore, rather than observing a step decrease in thickness as the temperature increases across a sharp T_m, a more gradual thinning is observed across the whole of the transition as a greater proportion of the bilayer exists in a fully fluid phase, showing excellent agreement between structural and thermodynamic data.

3.3. *Morphology and domains organisation in the lipid raft mimic by atomic force microscopy (AFM)*

AFM is a unique technique to visualize the lateral morphology of flat systems as supported membranes, and to detect the formation of phase separated domains with different nanometric thicknesses [104–107]. We have applied the technique to the protiated raft mimic SLB system in an attempt to visualise the temperature induced phase transition of the raft model and to verify the features and the evolution of the phase-separated, coexisting fluid and gel domains described by DSC. Additionally, for the sake of comparison, a DSC analysis of this raft model DMPC:SM:Chol 2:1:0.15 in molar ratios, in 100 mM NaCl buffer, (i.e. as in the same conditions of AFM measurements), was performed and is reported in Fig. S6. The measured thermogram had very similar shape to that referred to the deuterated model, but transition temperatures were slightly increased, by 1.5 °C, in agreement with the higher T_m of the DMPC compared to d_{54}DMPC.

Fig. 5 shows a series of 1.5 μm × 1.5 μm field size AFM images of the raft SLB while increasing the temperature at a rate of 0.02 °C/*s*, with 5 mins equilibrium time at each selected temperature step. As discussed in the SLB deposition process, it was first deposited at high temperature (40 °C), in the fluid phase; subsequently,the temperature was decreased down to 17 °C. At 17 °C in Fig. 5**a**, the SLB was almost complete with the presence of scattered pores, visible as dark spots. Zones of uncovered mica at 17 °C are consistent with the specific volume decrease and membrane thickening upon decreasing the SLB temperature from 40 °C. This is also in accordance with the reported NR analysis, where a higher solvent penetration was witnessed at 17 °C. Membrane pores deepness was exploited to evaluate the thickness of the raft in its gel phase [79,80,105,107]. A proper mask for all the pores in the SLB topographic map at 17 °C (Fig. 5**a**) was applied by Gwyddion software, obtaining an average SLB thickness equal to 51 ± 6 Å, in perfect agreement with the values of the 50 ± 1 Å and 52 ± 1 Å obtained from NR data analysis. The larger uncertainty, compared to NR data, can be likely attributed to the starting process of phase separation marked by the formation of small grooves, with typical depths around 2 Å, as shown in Fig. 6**a,b.**

Fig. 6**a** represents a zoom-in of 0.8 μm × 0.8 μm of the image Fig. 5**a**, aiming at highlighting the morphological details of the intricate network of extended, dark grooves delimiting islands of lighter color. Grooves appear as deep as about 2 Å, with respect to the broader islands, as shown from the line profile in Fig. 6**b**. Similar islands were observed in previous studies of SLB by AFM [79,105,107,108], and interpreted as lipids in the gel phase, in contrast with the darker grooves formed by lipids in the fluid phase.

By increasing the temperature of the SLB from 21 °C up to 25 °C (Fig. 5**b-d**), the grooves appeared to persist while the membrane pore defects were seen to shrink as the bilayer was laterally expanding on the mica. The grooves became more evident as deep as about 2.5 Å, upon increasing the SLB temperature to 25 °C, a value in the proximity of the melting of the less ordered phase, as observed by DSC. An increased value of T_m measured by AFM, is consistent with the different lipid conditions, i.e. solid-supported in AFM vs. bulk state in DSC: the presence of a solid interface is in fact stabilizing the phospholipid gel phase more than in bulk [104,107]. After melting, the system manifested the phase separation of the more-ordered gel-like SM/Chol enriched domains within the more fluid melted regions less enriched with SM/Chol. The broad melting process of the ordered gel domains, seen by DSC to occur up to 31 °C, is also confirmed by AFM for the surface-supported membrane. Details of the ordered gel domain height profile can be

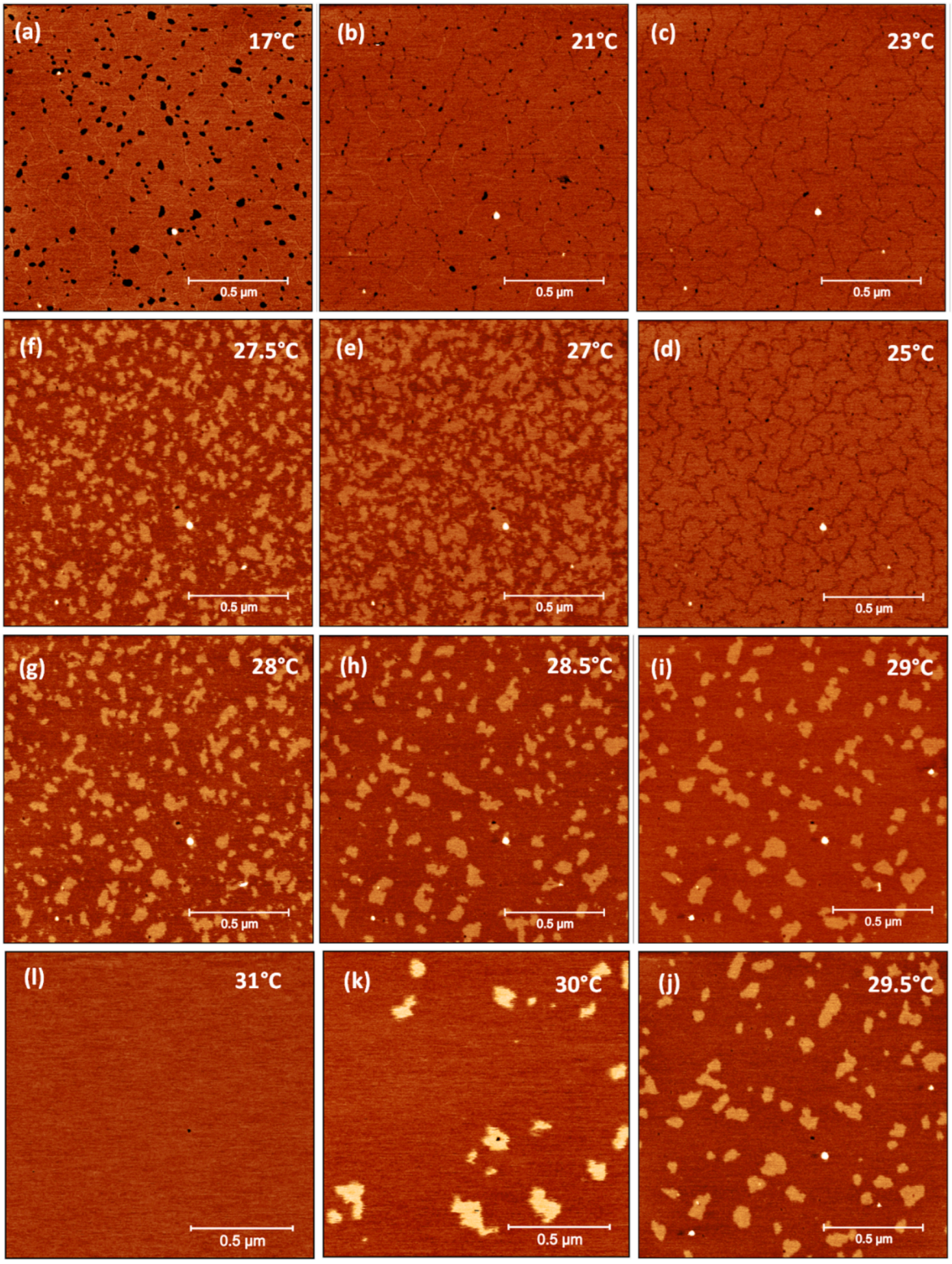

Fig. 5. AFM images of the formation of domains in the protiated raft SLB mimic. The membrane mimic presented here made of DMPC:SM:Chol; 2:1:0.15 M ratio, deposited on mica following the formation of the more ordered gel domains within the disordered phase, upon increasing the temperature: (a) 17 °C, (b) 21 °C, (c) 23 °C, (d) 25 °C, (e) 27 °C, (f) 27.5 °C, (g) 28 °C, (h) 28.5 °C, (i) 29 °C, (j) 29.5 °C, (k) 30 °C, (l) 31 °C, field size = 1.5x1.5 µm, scale bar: 0.5 µm. Detailed line profiles are shown in **Fig. S7.**

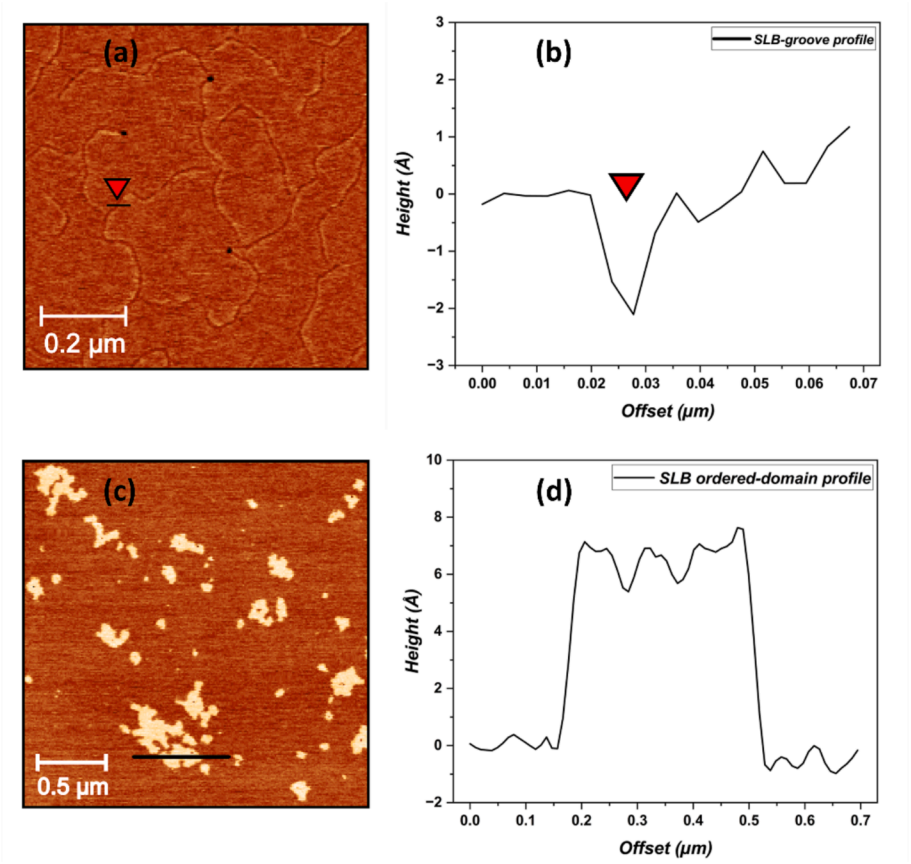

Fig. 6. AFM topography of the raft SLB at 17 °C (upper panels) and 29 °C (lower panels). Upper panel: scale bar: 0.2 µm, showing: (a) The appearance of grooves on the SLB surface, (b) The line profile of a groove. Lower panel: field size of 2x2 µm, scale bar: 0.5 µm showing: (c) The topography of the rafts ordered domains, (d) The line profile of a raft domain.

further seen in Fig. 6**c** which shows a topographic AFM image of the ordered domains at 29 °C and a corresponding domain line profile Fig. 6**d**, where the ordered gel domain is shown to have an average excess height of 6 ± 1Å.

Previous AFM imaging of supported DMPC bilayers [64] showed the formation of coexisting phases at varying temperatures during the phase transition. In our case, the ternary SLB mixture undergoes a two-step transition as seen by DSC, where the first sharp event is followed by an extended temperature range of coexisting fluid and gel phases pertaining to SM-depleted (less enriched) and SM-enriched domains, respectively. In our AFM experiments, the raft SLB temperature above 27 °C was changed in steps of 0.5 °C to monitor the subtle changes of the SLB morphology in this region.

Fig. 7 shows a superposition of the raft model thermogram obtained by the DSC measurement at the same conditions used for the AFM imaging, with the number and size of ordered domains observed by AFM along the melting phase transition. The full transition of DMPC into its liquid crystalline disordered phase was very broad, starting from 17 °C until 27 °C, and the ordered gel domains mainly rich in SM, only started to appear as thicker domains after the transition of the DMPC rich domains was concluded. Then, at increasing temperature, the ordered domains, less prone to melt, possibly move through the melted lipids and coalesce into larger regions, decreasing in number.

In the current raft model, the transition temperature of the DMPC region with the SM/Chol low enriched regions, measured by AFM, and the one in the MLV system, investigated by DSC, were only slightly shifted one with respect to the other. On the contrary, previous studies on the phase transition of pure DMPC showed that the melting of MLVs was not reproduced for supported membrane with a large shift of T_m to higher value, where a loss of cooperativity was suggested for the

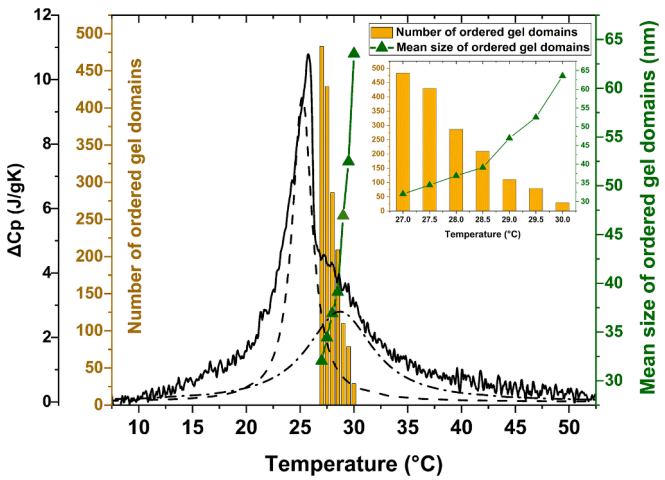

Fig. 7. DSC thermogram of the raft model made of DMPC:SM:Chol; 2:1:0.15 in molar ratio, in heating cycle, in comparison to the number and mean size of the ordered domains forming up in the SLB imaged by AFM while heating from 27 °C to 30 °C. The mean size of the ordered domains shown in green triangles and presented on the right Y-axis. The number of the ordered domains shown in yellow bars and presented on the yellow left Y-axis. The DSC thermogram in black solid line and presented on the black left Y-axis, while the dash line and the dot-dash line represent the peaks deconvolution of the thermogram into 2 peaks as discussed for the dRaft model in Fig. 4. The plot on the upper right side is a zooming into the mean size (green triangles) and number of ordered domains (yellow bars) at the selected temperatures from 27 °C to 30 °C presented in Fig. 5. (For interpretation of the references to color in this figure legend, the reader is referred to the web version of this article.)

supported system [105,107]. However, here the use of lipid ternary mixtures including cholesterol (raft SLB) makes the process more complex. Possibly, the creation of grooves that delimitate areas may enhance transition cooperativity within domains, alike in MLV raft. The use of lipid mixtures and ternary mixtures including cholesterol can indeed make the investigation of such phase shift behaviour more complex, since it depends on different parameters as the percentage of cholesterol used, the pH, or the rate of temperature change [107].

Further analysis of the AFM data is presented in Fig. 8, showing the difference between the area's percentages occupied by the ordered solid gel domains compared to the surrounding disordered liquid-crystalline phase upon increasing the temperature from 27 °C to 30 °C. The difference in area is represented in relation to the evolution of the excess difference in height of the ordered domains, with respect to the surrounding fluid phase thickness, which decreases at increasing temperatures. Area and number of the ordered gel domains have reduced significantly upon increasing the temperature of the SLB above its main transition. For instance, at 27 °C the SLB had around 53 % of its surface area arranged as ordered domains and this percentage decreased to only 6 % at 30 °C. SLB has fully melted into its liquid-crystalline disordered phase at 31 °C, acquiring a bilayer thickness of 44 Å as shown in Fig. S7 compared to the higher SLB thickness of 51 Å at 17 °C, in very good agreement with the reported NR results at the same temperatures.

4. Conclusions

In summary, we proposed and characterized here a solid raft membrane model composed of DMPC:SM:Chol in molar ratio 2:1:0.15, as a novel mimic to investigate the mechanism of uptake of vesicle/macromolecules. The chosen lipid mixture shows a coexistence of S_o and L_α phase-separated domains, the first ones being particularly relevant for intracellular transport, inter-organellar crosstalk and lipid transfer, among others. By analysing the system by means of complementary physical techniques, we gained a thorough understanding of its features and organisation.

In particular, DMPC allowed the use of neutron-based techniques due to its availability in deuterated form, and of DSC and AFM, thanks to its accessible T_m. SM, characterized by a higher T_m and longer acyl chains, giving rise to a broader melting in DMPC, into the ternary mixture gets preferentially packed with cholesterol, which is considered an essential driver of lipid raft formation. The low cholesterol ratio chosen here was found to be enough to achieve the required phase separation and confer the essential stability to the lipid domains, providing the required contrast between the coexisting phases, as observed by AFM. We imaged for the first time, the real-time formation of the lipid raft S_o domains in the ternary mixture upon temperature increase, showing the distinct morphological structure of our SLB below and above the T_m. These SLB showed a confirmed reproducibility with a very fast deposition kinetics on solid supports, and a high symmetry between the two leaflets, as shown by NR. SM increased the overall transition temperature and the broadness of the phase transition process of the binary and ternary mixtures, as shown by DSC, while cholesterol has driven the required phase separation, as observed by the appearance of a new peak in the DMPC/Chol binary and DMPC/SM/Chol ternary mixtures thermograms. AFM investigation of membrane morphology through the phase transition, revealed the intricate structure of the raft SLB in the gel phase, where grooves and indentations were witnessed as starting lines directing the assembly of the S_o domains within the surrounding disordered fluid phase.

This study thus positively impacts the field of membrane models and lipid rafts research by opening to the opportunity of mimicking S_o domains and exploring their functionality in addition to the usual studies already performed on the L_o domains.

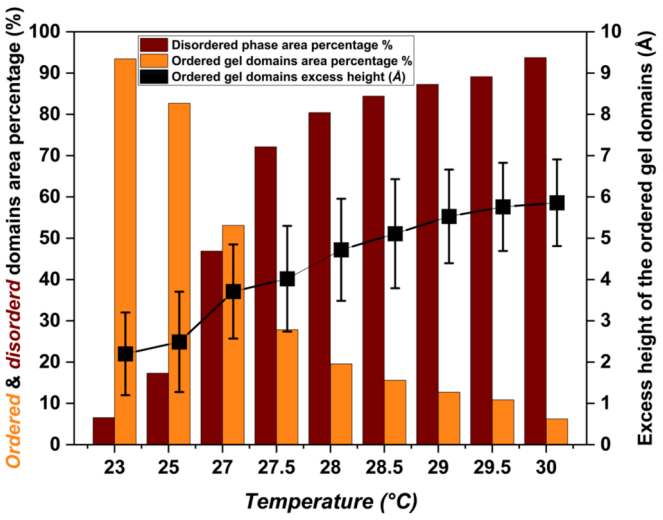

Fig. 8. A comparison of the domains area percentage for the AFM images of the protiated raft model at different temperatures. DMPC:SM:Chol; 2:1:0.15 model at the temperature range 27 °C–30 °C shown in Fig. 5, showing the changes in the area percentages of the ordered and disordered phases and the corresponding changes of the thickness of disordered and ordered membrane domains.

CRediT authorship contribution statement

Sally Helmy: Writing – review & editing, Writing – original draft, Visualization, Methodology, Investigation, Formal analysis, Data curation. **Paola Brocca:** Writing – review & editing, Writing – original draft, Supervision. **Alexandros Koutsioubas:** Writing – review & editing, Software, Investigation. **Stephen C.L. Hall:** Writing – review & editing, Resources, Investigation, Data curation. **Luca Puricelli:** Writing – review & editing, Investigation, Data curation. **Pietro Parisse:** Writing – review & editing, Supervision, Resources. **Loredana Casalis:** Writing – review & editing, Writing – original draft, Supervision, Resources. **Valeria Rondelli:** Writing – review & editing, Writing – original draft, Supervision, Resources, Project administration, Investigation, Funding acquisition, Conceptualization.

Funding

Sally Helmy was funded by a full PhD scholarship (mission 2019/2020) from the cultural affairs and missions sector of the Ministry of Higher Education in Egypt. This work has received funding from the Italian Ministry of University and Research, PRIN2020 project n. 2020MHL8S9 "MITHOS" (to VR). This research was funded by "Next Generation EU Missione 4 Componente 2, for the project n. P2022J2ZC2 (to VR-CUP: G53D23007030001- and PP) and project n. 20223SM7T2 to VR-CUP: G53D23003300001. This work has also been partially funded by the European Union – NextGenerationEU within the project PNRR "PRP@CERIC" IR0000028.

Declaration of competing interest

The authors declare that they have no known competing financial interests or personal relationships that could have appeared to influence the work reported in this paper.

Acknowledgments

This work benefited from the use of the Offspec vertical neutron reflectometer beamtime; DOI: 10.5286/ISIS.E.RB2210183 at the ISIS Neutron and Muon Source, Oxfordshire, UK. This work benefited from the use of the anaklasis, an open-source Python3 scripts provided by

Alexandros Koutsioubas.

Appendix A. Supplementary data

Supplementary data to this article can be found online at https://doi.org/10.1016/j.jcis.2025.137333.

Data availability

Data will be made available on request.

References

[1] T. Fujimoto, I. Parmryd, Interleaflet coupling, pinning, and leaflet asymmetry—major players in plasma membrane nanodomain formation, Front. Cell Dev. Biol. 4 (2017) 155, https://doi.org/10.3389/fcell.2016.00155.

[2] L.J. Pike, The challenge of lipid rafts, J. Lipid Res. 50 (2009) S323–S328, https://doi.org/10.1194/jlr.R800040-JLR200.

[3] G. van Meer, Dynamic transbilayer lipid asymmetry, Cold Spring Harb. Perspect. Biol. 3 (2011) a004671, https://doi.org/10.1101/cshperspect.a004671.

[4] T. Róg, I. Vattulainen, Cholesterol, sphingolipids, and glycolipids: what do we know about their role in raft-like membranes? Chem. Phys. Lip. 184 (2014) 82–104, https://doi.org/10.1016/j.chemphyslip.2014.10.004.

[5] M.L. Kraft, Sphingolipid organization in the plasma membrane and the mechanisms that influence it, Front. Cell Dev. Biol. 4 (2017) 154, https://doi.org/10.3389/fcell.2016.00154.

[6] J. Yu, D.A. Fischman, T.L. Steck, Selective solubilization of proteins and phospholipids from red blood cell membranes by nonionic detergents, J. Supramol. Struct. 1 (1973) 233–248, https://doi.org/10.1002/jss.400010308.

[7] D. Lingwood, K. Simons, Lipid rafts as a membrane-organizing principle, Science 327 (2010) (1979) 46–50, https://doi.org/10.1126/science:1174621.

[8] D. Lingwood, H.-J. Kaiser, I. Levental, K. Simons, Lipid rafts as functional heterogeneity in cell membranes, Biochem. Soc. Trans. 37 (2009) 955–960, https://doi.org/10.1042/BST0370955.

[9] B.P. Head, H.H. Patel, P.A. Insel, Interaction of membrane/lipid rafts with the cytoskeleton: impact on signaling and function: membrane/lipid rafts, mediators of cytoskeletal arrangement and cell signaling, Biochim. Biophys. Acta (BBA)-Biomembr. 1838 (2014) 532–545, https://doi.org/10.1016/j.bbamem.2013.07.018.

[10] K. Simons, W.L.C. Vaz, Model systems, lipid rafts, and cell membranes, Annu. Rev. Biophys. Biomol. Struct. 33 (2004) 269–295, https://doi.org/10.1146/annurev.biophys.32.110601.141803.

[11] M.B. Sankaram, T.E. Thompson, Cholesterol-induced fluid-phase immiscibility in membranes, Proc. Natl. Acad. Sci. 88 (1991) 8686–8690, https://doi.org/10.1073/pnas.88.19.8686.

[12] H. Ohvo-Rekilä, B. Ramstedt, P. Leppimäki, J.P. Slotte, Cholesterol interactions with phospholipids in membranes, Prog. Lipid Res. 41 (2002) 66–97, https://doi.org/10.1016/S0163-7827(01)00020-0.

[13] A.Y. Dunina-Barkovskaya, Cell membrane cholesterol and regulation of cellular processes: new and the same old thing, Biochem. (Mosc.) Suppl. Ser. A Membr. Cell Biol. 18 (2024) 224–240, https://doi.org/10.1134/S1990747824700223.

[14] R. Lipowsky, Domains and rafts in membranes–Hidden dimensions of selforganization, J. Biol. Phys. 28 (2002) 195–210, https://doi.org/10.1023/A:1019994628793.

[15] J. Zhang, A. Pekosz, R.A. Lamb, Influenza virus assembly and lipid raft microdomains: a role for the cytoplasmic tails of the spike glycoproteins, J. Virol. 74 (2000) 4634–4644, https://doi.org/10.1128/jvi.74.10.4634-4644.2000.

[16] T. Harder, P. Scheiffele, P. Verkade, K. Simons, Lipid domain structure of the plasma membrane revealed by patching of membrane components, J. Cell Biol. 141 (1998) 929–942, https://doi.org/10.1083/jcb.141.4.929.

[17] T. Izard, Environmental and their disruption of integrin signaling in lipid rafts, Bioessays (2025), https://doi.org/10.1002/bies.202400276.

[18] R. Virk, K. Cook, A. Cavazos, S.R. Wassall, K.M. Gowdy, S.R. Shaikh, How membrane phospholipids containing long-chain polyunsaturated fatty acids and their oxidation products orchestrate lipid raft dynamics to control inflammation, J. Nutr. 154 (2024) 2862–2870, https://doi.org/10.1016/j.tjnut.2024.07.015.

[19] B. Viljetić, S. Blažetić, I. Labak, V. Ivić, M. Zjalić, M. Heffer, M. Balog, Lipid rafts: the maestros of normal brain development, Biomolecules 14 (2024) 362, https://doi.org/10.3390/biom14030362.

[20] K. Gaus, E. Gratton, E.P.W. Kable, A.S. Jones, I. Gelissen, L. Kritharides, W. Jessup, Visualizing lipid structure and raft domains in living cells with two-photon microscopy, Proc. Natl. Acad. Sci. 100 (2003) 15554–15559, https://doi.org/10.1073/pnas.2534386100.

[21] J.A. Nieto-Garai, M. Lorizate, F.-X. Contreras, Shedding light on membrane rafts structure and dynamics in living cells, Biochim. Biophys. Acta (BBA)-Biomembr. 1864 (2022) 183813, https://doi.org/10.1016/j.bbamem.2021.183813.

[22] O. Bakht, P. Pathak, E. London, Effect of the structure of lipids favoring disordered domain formation on the stability of cholesterol-containing ordered domains (lipid rafts): identification of multiple raft-stabilization mechanisms, Biophys. J . 93 (2007) 4307–4318, https://doi.org/10.1529/biophysj.107.114967.

[23] C. Dietrich, Z.N. Volovyk, M. Levi, N.L. Thompson, K. Jacobson, Partitioning of Thy-1, GM1, and cross-linked phospholipid analogs into lipid rafts reconstituted in supported model membrane monolayers, Proc. Natl. Acad. Sci. 98 (2001) 10642–10647, https://doi.org/10.1073/pnas.191168698.

[24] Y. Wang, Y. Palzhanov, A. Quaini, M. Olshanskii, S. Majd, Lipid domain coarsening and fluidity in multicomponent lipid vesicles: a continuum based model and its experimental validation, Biochim. Biophys. Acta (BBA)-Biomembr. 1864 (2022) 183898, https://doi.org/10.1016/j.bbamem.2022.183898.

[25] P.E. Milhiet, M.-C. Giocondi, C. Le Grimellec, AFM imaging of lipid domains in model membranes, Sci. World J. 3 (2003) 59–74, https://doi.org/10.1100/tsw.2003.12.

[26] R.M. Henderson, J.M. Edwardson, N.A. Geisse, D.E. Saslowsky, Lipid rafts: feeling is believing, Physiology 19 (2004) 39–43, https://doi.org/10.1152/nips.01505.2003.

[27] J. Pencer, T. Mills, V. Anghel, S. Krueger, R.M. Epand, J. Katsaras, Detection of submicron-sized raft-like domains in membranes by small-angle neutron scattering, Euro. Phys. J. E 18 (2005) 447–458, https://doi.org/10.1140/epje/e2005-00046-5.

[28] D. Ahmadi, K.C. Thompson, V. García Sakai, R. Schweins, M. Moulin, M. Haertlein, G.A. Strohmeier, H. Pichler, V.T. Forsyth, D.J. Barlow, Nanoscale structure and dynamics of model membrane lipid raft systems, studied by neutron scattering methods, Front. Phys. 10 (2022) 864746, https://doi.org/10.3389/fphy.2022.864746.

[29] M. Hirai, H. Hirai, M. Koizumi, K. Kasahara, K. Yuyama, N. Suzuki, Structure of raft-model membrane by using the inverse contrast variation neutron scattering method, Phys. B Condens. Matter 385 (2006) 868–870, https://doi.org/10.1016/j.physb.2006.05.129.

[30] J. Pan, F.A. Heberle, R.S. Petruzielo, J. Katsaras, Using small-angle neutron scattering to detect nanoscopic lipid domains, Chem. Phys. Lipids 170 (2013) 19–32, https://doi.org/10.1016/j.chemphyslip.2013.02.012.

[31] P. Sengupta, B. Baird, D. Holowka, Lipid rafts, fluid/fluid phase separation, and their relevance to plasma membrane structure and function, Semin. Cell Dev. Biol. 18 (5) (2007) 583–590, https://doi.org/10.1016/j.semcdb.2007.07.010.

[32] E.L. Elson, E. Fried, J.E. Dolbow, G.M. Genin, Phase separation in biological membranes: integration of theory and experiment, Annu. Rev. Biophys. 39 (2010) 207–226, https://doi.org/10.1146/annurev.biophys.093008.131238.

[33] I. Levental, K.R. Levental, F.A. Heberle, Lipid rafts: controversies resolved, mysteries remain, Trends Cell Biol. 30 (2020) 341–353, https://doi.org/10.1016/j.tcb.2020.01.009.

[34] J.-S. Bae, L. Yang, A.R. Rezaie, Receptors of the protein C activation and activated protein C signaling pathways are colocalized in lipid rafts of endothelial cells, Proc. Natl. Acad. Sci. 104 (2007) 2867–2872, https://doi.org/10.1073/pnas.0611493104.

[35] F. Perissinotto, V. Rondelli, B. Senigagliesi, P. Brocca, L. Almásy, L. Bottyán, D. G. Merkel, H. Amenitsch, B. Sartori, K. Pachler, Structural insights into fusion mechanisms of small extracellular vesicles with model plasma membranes, Nanoscale 13 (2021) 5224–5233, https://doi.org/10.1039/D0NR09075A.

[36] F. Perissinotto, C. Stani, E. De Cecco, L. Vaccari, V. Rondelli, P. Posocco, P. Parisse, D. Scaini, G. Legname, L. Casalis, Iron-mediated interaction of alpha synuclein with lipid raft model membranes, Nanoscale 12 (2020) 7631–7640, https://doi.org/10.1039/D0NR00287A.

[37] H. Tsuchiya, M. Mizogami, Interaction of drugs with lipid raft membrane domains as a possible target, Drug Target Insights 14 (2020) 34, https://doi.org/10.33393/dti.2020.2185.

[38] A.J. García-Sáez, S. Chiantia, P. Schwille, Effect of line tension on the lateral organization of lipid membranes, J. Biol. Chem. 282 (2007) 33537–33544, https://doi.org/10.1074/jbc.M706162200.

[39] S.L. Veatch, S.L. Keller, Miscibility phase diagrams of giant vesicles containing sphingomyelin, PhysRevLett 94 (2005) 148101, https://doi.org/10.1103/PhysRevLett.94.148101.

[40] S.J. Attwood, Y. Choi, Z. Leonenko, Preparation of DOPC and DPPC supported planar lipid bilayers for atomic force microscopy and atomic force spectroscopy, Int. J. Mol. Sci. 14 (2013) 3514–3539, https://doi.org/10.3390/ijms14023514.

[41] K.J. Fritzsching, J. Kim, G.P. Holland, Probing lipid–cholesterol interactions in DOPC/eSM/Chol and DOPC/DPPC/Chol model lipid rafts with DSC and 13C solid-state NMR, Biochim. Biophys. Acta (BBA)-Biomembr. 1828 (2013) 1889–1898, https://doi.org/10.1016/j.bbamem.2013.03.028.

[42] R.F.M. de Almeida, E. Joly, Crystallization around solid-like nanosized docks can explain the specificity, diversity, and stability of membrane microdomains, Front. Plant Sci. 5 (2014) 72, https://doi.org/10.3389/fpls.2014.00072.

[43] H.-Y. Wang, D. Bharti, I. Levental, Membrane heterogeneity beyond the plasma membrane, Front. Cell Dev. Biol. 8 (2020) 580814, https://doi.org/10.3389/fcell.2020.580814.

[44] L.J. Pike, Rafts defined: a report on the keystone symposium on lipid rafts and cell function, J. Lipid Res. 47 (2006) 1597–1598, https://doi.org/10.1194/jlr.E600002-JLR200.

[45] A. Kusumi, K. Suzuki, Toward understanding the dynamics of membrane-raft-based molecular interactions, Biochim. Biophys. Acta (BBA)-Mole. Cell Res. 1746 (2005) 234–251, https://doi.org/10.1016/j.bbamcr.2005.10.001.

[46] D.V. Nicolau Jr, K. Burrage, R.G. Parton, J.F. Hancock, Identifying optimal lipid raft characteristics required to promote nanoscale protein-protein interactions on the plasma membrane, Mol. Cell Biol. 26 (2006) 313–323, https://doi.org/10.1128/MCB.26.1.313-323.2006.

[47] E.C.I. Veerman, M. Valentijn-Benz, K. Nazmi, A.L.A. Ruissen, E. Walgreen-Weterings, J. van Marle, A.B. Doust, W. van't Hof, J.G.M. Bolscher, A.V. N. Amerongen, Energy depletion protects Candida albicans against antimicrobial

peptides by rigidifying its cell membrane, J. Biol. Chem. 282 (2007) 18831–18841, https://doi.org/10.1074/jbc.M610555200.
[48] M.-N. Vaultier, C. Cantrel, C. Vergnolle, A.-M. Justin, C. Demandre, G. Benhassaine-Kesri, D. Çiçek, A. Zachowski, E. Ruelland, Desaturase mutants reveal that membrane rigidification acts as a cold perception mechanism upstream of the diacylglycerol kinase pathway in Arabidopsis cells, FEBS Lett. 580 (2006) 4218–4223, https://doi.org/10.1016/j.febslet.2006.06.083.
[49] M. Caffrey, J. Hogan, LIPIDAT: a database of lipid phase transition temperatures and enthalpy changes. DMPC data subset analysis, Chem. Phys. Lip. 61 (1992) 1–109, https://doi.org/10.1016/0009-3084(92)90002-7.
[50] D. Drabik, G. Chodaczek, S. Kraszewski, M. Langner, Mechanical properties determination of DMPC, DPPC, DSPC, and HSPC solid-ordered bilayers, Langmuir 36 (2020) 3826–3835, https://doi.org/10.1021/acs.langmuir.0c00475.
[51] M. Grava, S. Helmy, M. Gimona, P. Parisse, L. Casalis, P. Brocca, V. Rondelli, Calorimetry of extracellular vesicles fusion to single phospholipid membrane, Biomol. Concepts 13 (2022) 148–155, https://doi.org/10.1515/bmc-2022-0011.
[52] P. Jurczak, K. Szutkowski, S. Lach, S. Jurga, P. Czaplewska, A. Szymanska, I. Zhukov, DMPC phospholipid bilayer as a potential interface for human cystatin C oligomerization: analysis of protein-liposome interactions using NMR spectroscopy, Membranes (Basel) 11 (2020) 13, https://doi.org/10.3390/membranes11010013.
[53] R.N. McElhaney, The use of differential scanning calorimetry and differential thermal analysis in studies of model and biological membranes, Chem. Phys. Lipids 30 (1982) 229–259, https://doi.org/10.1016/0009-3084(82)90053-6.
[54] T. Heimburg, Mechanical aspects of membrane thermodynamics. Estimation of the mechanical properties of lipid membranes close to the chain melting transition from calorimetry, Biochim. Biophys. Acta (BBA)-Biomembr. 1415 (1998) 147–162, https://doi.org/10.1016/S0005-2736(98)00189-8.
[55] T.K.M. Nyholm, M. Nylund, J.P. Slotte, A calorimetric study of binary mixtures of dihydrosphingomyelin and sterols, sphingomyelin, or phosphatidylcholine, Biophys. J . 84 (2003) 3138–3146, https://doi.org/10.1016/S0006-3495(03)70038-1.
[56] P. Brocca, L. Cantù, M. Corti, E. Del Favero, S. Motta, M.C. Nodari, DC13PC bilayers from anomalous swelling to main transition: an X-ray scattering investigation, J. Colloid Interface Sci. 312 (2007) 34–41, https://doi.org/10.1016/j.jcis.2006.12.067.
[57] O. Enders, A. Ngezahayo, M. Wiechmann, F. Leisten, H.-A. Kolb, Structural calorimetry of main transition of supported DMPC bilayers by temperature-controlled AFM, Biophys. J . 87 (2004) 2522–2531, https://doi.org/10.1529/biophysj.104.040105.
[58] P. Brocca, L. Cantu, M. Corti, E. Del Favero, S. Motta, M.C. Nodari, Curved single-bilayers in the region of the anomalous swelling: effect of curvature and chain length, Colloids Surf. A Physicochem. Eng. Asp 291 (2006) 63–68, https://doi.org/10.1016/j.colsurfa.2006.08.014.
[59] J. Drazenovic, H. Wang, K. Roth, J. Zhang, S. Ahmed, Y. Chen, G. Bothun, S. L. Wunder, Effect of lamellarity and size on calorimetric phase transitions in single component phosphatidylcholine vesicles, Biochim. Biophys. Acta (BBA)-Biomembr. 1848 (2015) 532–543, https://doi.org/10.1016/j.bbamem.2014.10.003.
[60] B. Klajnert, J. Janiszewska, Z. Urbanczyk-Lipkowska, M. Bryszewska, R.M. Epand, DSC studies on interactions between low molecular mass peptide dendrimers and model lipid membranes, Int. J. Pharm. 327 (2006) 145–152, https://doi.org/10.1016/j.ijpharm.2006.07.018.
[61] R.N. McElhaney, Differential scanning calorimetric studies of lipid-protein interactions in model membrane systems, Biochim. Biophys. Acta Biomembr. 864 (3-4) (1986) 361–421, https://doi.org/10.1016/0304-4157(86)90004-3.
[62] I. Sahin, Ç. Ceylan, O. Bayraktar, Ruscogenin interacts with DPPC and DPPG model membranes and increases the membrane fluidity: FTIR and DSC studies, Arch. Biochem. Biophys. 733 (2023) 109481, https://doi.org/10.1016/j.abb.2022.109481.
[63] V. Rondelli, A. Koutsioubas, E. Di Cola, G. Fragneto, I. Grillo, E. Del Favero, L. Colombo, L. Cantù, P. Brocca, M. Salmona, Dysmyelination and glycolipid interference caused by phenylalanine in phenylketonuria, Int. J. Biol. Macromol. 221 (2022) 784–795, https://doi.org/10.1016/j.ijbiomac.2022.09.062.
[64] F. Tokumasu, A.J. Jin, J.A. Dvorak, Lipid membrane phase behaviour elucidated in real time by controlled environment atomic force microscopy, Microscopy 51 (2002) 1–9, https://doi.org/10.1093/jmicro/51.1.1.
[65] A. Alessandrini, P. Facci, Unraveling lipid/protein interaction in model lipid bilayers by atomic force microscopy, J. Mol. Recogn. 24 (2011) 387–396, https://doi.org/10.1002/jmr.1083.
[66] F. Perissinotto, V. Rondelli, P. Parisse, N. Tormena, A. Zunino, L. Almásy, D. G. Merkel, L. Bottyán, S. Sajti, L. Casalis, GM1 Ganglioside role in the interaction of Alpha-synuclein with lipid membranes: morphology and structure, Biophys. Chem. 255 (2019) 106272, https://doi.org/10.1016/j.bpc.2019.106272.
[67] C. Paba, V. Dorigo, B. Senigagliesi, N. Tormena, P. Parisse, K. Voitchovsky, L. Casalis, Lipid bilayer fluidity and degree of order regulates small EVs adsorption on model cell membrane, J. Colloid Interface Sci. 652 (2023) 1937–1943, https://doi.org/10.1016/j.jcis.2023.08.117.
[68] G. Fragneto, Neutrons and model membranes, Eur. Phys. J. Spec. Top 213 (2012) 327–342, https://doi.org/10.1140/epjst/e2012-01680-5.
[69] V. Rondelli, E. Del Favero, S. Motta, L. Cantù, G. Fragneto, P. Brocca, Neutrons for rafts, rafts for neutrons, Euro. Phys. J. E 36 (2013) 1–8, https://doi.org/10.1140/epje/i2013-13073-4.
[70] V. Rondelli, P. Brocca, S. Motta, M. Messa, L. Colombo, M. Salmona, G. Fragneto, L. Cantù, E. Del Favero, Amyloidβ Peptides in interaction with raft-mime model membranes: a neutron reflectivity insight, Sci. Rep. 6 (2016) 20997, https://doi.org/10.1038/srep20997.
[71] V. Rondelli, P. Brocca, N. Tranquilli, G. Fragneto, E. Del Favero, L. Cantù, Building a biomimetic membrane for neutron reflectivity investigation: complexity, asymmetry and contrast, Biophys. Chem. 229 (2017) 135–141, https://doi.org/10.1016/j.bpc.2017.04.011.
[72] G.J. Hardy, R. Nayak, S. Zauscher, Model cell membranes: Techniques to form complex biomimetic supported lipid bilayers via vesicle fusion, Curr. Opin. Colloid Interf. Sci. 18 (2013) 448–458, https://doi.org/10.1016/j.cocis.2013.06.004.
[73] E. Reimhult, F. Höök, B. Kasemo, Temperature dependence of formation of a supported phospholipid bilayer from vesicles on SiO 2, PhysRevE 66 (2002) 051905, https://doi.org/10.1103/PhysRevE.66.051905.
[74] R. Pynn, S.M. Baker, G. Smith, M. Fitzsimmons, Off-specular scattering in neutron reflectometry, J. Neutron Res. 7 (1999) 139–158, https://doi.org/10.1080/10238169908200113.
[75] A. Koutsioubas, anaklasis: a compact software package for model-based analysis of specular neutron and X-ray reflectometry data sets, J. Appl. Cryst. 54 (2021) 1857–1866, https://doi.org/10.1107/S1600576721009262.
[76] G. Fragneto, R.K. Thomas, A.R. Rennie, J. Penfold, Neutron reflection study of bovine β-casein adsorbed on OTS self-assembled monolayers, Science 267 (1995) (1979) 657–660, https://doi.org/10.1126/science:7839141.
[77] H.P. Wacklin, Neutron reflection from supported lipid membranes, Curr. Opin. ColloidInterf. Sci. 15 (2010) 445–454, https://doi.org/10.1016/j.cocis.2010.05.008.
[78] G. Salvetti, C. Cardelli, C. Ferrari, E. Tombari, A modulated adiabatic scanning calorimeter (MASC), Thermochim. Acta 364 (2000) 11–22, https://doi.org/10.1016/S0040-6031(00)00645-6.
[79] F. Tokumasu, A.J. Jin, G.W. Feigenson, J.A. Dvorak, Atomic force microscopy of nanometric liposome adsorption and nanoscopic membrane domain formation, Ultramicroscopy 97 (2003) 217–227, https://doi.org/10.1016/S0304-3991(03)00046-9.
[80] Z. Al-Rekabi, S. Contera, Multifrequency AFM reveals lipid membrane mechanical properties and the effect of cholesterol in modulating viscoelasticity, Proc. Natl. Acad. Sci. 115 (2018) 2658–2663, https://doi.org/10.1073/pnas.1719065115.
[81] A.I. Greenwood, S. Tristram-Nagle, J.F. Nagle, Partial molecular volumes of lipids and cholesterol, Chem. Phys. Lipids 143 (2006) 1–10, https://doi.org/10.1016/j.chemphyslip.2006.04.002.
[82] J.F. Nagle, R.M. Venable, E. Maroclo-Kemmerling, S. Tristram-Nagle, P.E. Harper, R.W. Pastor, Revisiting volumes of lipid components in bilayers, J. Phys. Chem. B 123 (2019) 2697–2709, https://doi.org/10.1021/acs.jpcb.8b12010.
[83] A. Watts, D. Marsh, P.F. Knowles, Characterization of dimyristoylphosphatidylcholine vesicles and their dimensional changes through the phase transition: molecular control of membrane morphology, Biochemistry 17 (1978) 1792–1801, https://doi.org/10.1021/bi00602a034.
[84] M. Wadsater, J.B. Simonsen, T. Lauridsen, E.G. Tveten, P. Naur, T. Bjørnholm, H. Wacklin, K. Mortensen, L. Arleth, R. Feidenhans'l, Aligning nanodiscs at the air–water interface, a neutron reflectivity study, Langmuir 27 (2011) 15065–15073, https://doi.org/10.1021/la203100n.
[85] R. Tero, Substrate effects on the formation process, structure and physicochemical properties of supported lipid bilayers, Materials 5 (2012) 2658–2680, https://doi.org/10.3390/ma5122658.
[86] J.F. Nagle, S. Tristram-Nagle, Structure of lipid bilayers, Biochim. Biophys. Acta (BBA)-Rev. Biomembr. 1469 (2000) 159–195, https://doi.org/10.1016/S0304-4157(00)00016-2.
[87] V. Rondelli, G. Fragneto, S. Motta, E. Del Favero, L. Cantù, Reflectivity from floating bilayers: can we keep the structural asymmetry?, in: J Phys Conf Ser, IOP Publishing, 2012, p. 012083. doi: 10.1088/1742-6596/340/1/012083.
[88] V. Rondelli, A. Koutsioubas, J. Pršić, E. Deboever, J.-M. Crowet, L. Lins, M. Deleu, Sitosterol and glucosylceramide cooperative transversal and lateral uneven distribution in plant membranes, Sci. Rep. 11 (2021) 21618, https://doi.org/10.1038/s41598-021-00696-7.
[89] G. Bryant, M.B. Taylor, T.A. Darwish, A.M. Krause-Heuer, B. Kent, C.J. Garvey, Effect of deuteration on the phase behaviour and structure of lamellar phases of phosphatidylcholines–deuterated lipids as proxies for the physical properties of native bilayers, Colloids Surf. B Biointerf. 177 (2019) 196–203, https://doi.org/10.1016/j.colsurfb.2019.01.040.
[90] J. Lemmich, T. Hønger, K. Mortensen, J.H. Ipsen, R. Bauer, O.G. Mouritsen, Solutes in small amounts provide for lipid-bilayer softness: cholesterol, short-chain lipids, and bola lipids, Eur. Biophys. J. 25 (1996) 61–65, https://doi.org/10.1007/s002490050018.
[91] R. Koynova, M. Caffrey, Phases and phase transitions of the phosphatidylcholines, Biochimica et Biophysica Acta (BBA)-Rev. Biomembr. 1376 (1998) 91–145, https://doi.org/10.1016/S0304-4157(98)00006-9.
[92] Z. Arsov, E.J. González-Ramírez, F.M. Goñi, S. Tristram-Nagle, J.F. Nagle, Phase behavior of palmitoyl and egg sphingomyelin, Chem. Phys. Lipids 213 (2018) 102–110, https://doi.org/10.1016/j.chemphyslip.2018.03.003.
[93] P. Losada-Pérez, N. Mertens, B. de Medio-Vasconcelos, E. Slenders, J. Leys, M. Peeters, B. Van Grinsven, J. Gruber, C. Glorieux, H. Pfeiffer, Phase transitions of binary lipid mixtures: a combined study by adiabatic scanning calorimetry and quartz crystal microbalance with dissipation monitoring, Adv. Condens. Matter Phys. 2015 (2015) 479318, https://doi.org/10.1155/2015/479318.
[94] U. Ros, M.A. Edwards, R.F. Epand, M.E. Lanio, S. Schreier, C.M. Yip, C. Alvarez, R.M. Epand, The sticholysin family of pore-forming toxins induces the mixing of lipids in membrane domains, Biochim. Biophys. Acta (BBA)-Biomembr. 1828 (2013) 2757–2762, https://doi.org/10.1016/j.bbamem.2013.08.001.

[95] P.F.F. Almeida, W.L.C. Vaz, T.E. Thompson, Lateral diffusion in the liquid phases of dimyristoylphosphatidylcholine/cholesterol lipid bilayers: a free volume analysis, Biochemistry 31 (1992) 6739–6747, https://doi.org/10.1021/bi00144a013.
[96] C.L. Armstrong, D. Marquardt, H. Dies, N. Kučerka, Z. Yamani, T.A. Harroun, J. Katsaras, A.-C. Shi, M.C. Rheinstädter, The observation of highly ordered domains in membranes with cholesterol, PLoS One 8 (2013) e66162, https://doi.org/10.1371/journal.pone.0066162.
[97] A. Pokorny, P.F.F. Almeida, E.C.C. Melo, W.L.C. Vaz, Kinetics of amphiphile association with two-phase lipid bilayer vesicles, Biophys. J. 78 (2000) 267–280, https://doi.org/10.1016/S0006-3495(00)76590-8.
[98] Estep, T.N. Mountcastle, D.B. Biltonen, R.L.Te. Thompson, Studies on the anomalous thermotropic behavior of aqueous dispersions of dipalmitoylphosphatidylcholine-cholesterol mixtures, Biochemistry 17 (1978) 1984–1989, https://doi.org/10.1021/bi00603a029.
[99] J. Lemmich, K. Mortensen, J.H. Ipsen, T. Hønger, R. Bauer, O.G. Mouritsen, The effect of cholesterol in small amounts on lipid-bilayer softness in the region of the main phase transition, Eur. Biophys. J. 25 (1997) 293–304, https://doi.org/10.1007/s002490050041.
[100] T.P.W. McMullen, R.N. McElhaney, New aspects of the interaction of cholesterol with dipalmitoylphosphatidylcholine bilayers as revealed by high-sensitivity differential scanning calorimetry, Biochim. Biophys. Acta (BBA)-Biomembr. 1234 (1995) 90–98, https://doi.org/10.1016/0005-2736(94)00266-R.
[101] N. Kahya, D. Scherfeld, P. Schwille, Differential lipid packing abilities and dynamics in giant unilamellar vesicles composed of short-chain saturated glycerol-phospholipids, sphingomyelin and cholesterol, Chem. Phys. Lipids 135 (2005) 169–180, https://doi.org/10.1016/j.chemphyslip.2005.02.013.
[102] G.W. Feigenson, Phase diagrams and lipid domains in multicomponent lipid bilayer mixtures, Biochim. Biophys. Acta Biomembr. 1788 (2009) 47–52, https://doi.org/10.1016/j.bbamem.2008.08.014.
[103] M. Lönnfors, J.P.F. Doux, J.A. Killian, T.K.M. Nyholm, J.P. Slotte, Sterols have higher affinity for sphingomyelin than for phosphatidylcholine bilayers even at equal acyl-chain order, Biophys. J . 100 (2011) 2633–2641, https://doi.org/10.1016/j.bpj.2011.03.066.
[104] R.S. Gunderson, A.R. Honerkamp-Smith, Liquid-liquid phase transition temperatures increase when lipid bilayers are supported on glass, Biochim. Biophys. Acta (BBA)-Biomembr. 1860 (2018) 1965–1971, https://doi.org/10.1016/j.bbamem.2018.05.001.
[105] A. Charrier, F. Thibaudau, Main phase transitions in supported lipid single-bilayer, Biophys. J . 89 (2005) 1094–1101, https://doi.org/10.1529/biophysj.105.062463.
[106] S.D. Connell, D.A. Smith, The atomic force microscope as a tool for studying phase separation in lipid membranes, Mol. Membr. Biol. 23 (2006) 17–28, https://doi.org/10.1080/09687860500501158.
[107] A. Alessandrini, P. Facci, Phase transitions in supported lipid bilayers studied by AFM, Soft Matter 10 (2014) 7145–7164, https://doi.org/10.1039/C4SM01104J.
[108] M.-C. Giocondi, C. Le Grimellec, Temperature dependence of the surface topography in dimyristoylphosphatidylcholine/distearoylphosphatidylcholine multibilayers, Biophys. J. 86 (2004) 2218–2230, https://doi.org/10.1016/S0006-3495(04)74280-0.